Dyes and Pigments 206 (2022) 110566

Contents lists available at ScienceDirect

Dyes and Pigments

journal homepage: www.elsevier.com/locate/dyepig

Pyranylidene/trifluoromethylbenzoic acid-based chromophores for dye-sensitized solar cells

Raquel Royo, Amelia Domínguez-Celorrio, Santiago Franco **, Raquel Andreu *, Jesús Orduna

Instituto de Nanociencia y Materiales de Aragón (INMA)-Departamento de Química Orgánica, CSIC-Universidad de Zaragoza, Zaragoza, 50009, Spain

ARTICLE INFO

Keywords:
D-π-A dyes
4*H*-pyranylidene
DSSC
Trifluoromethyl group

ABSTRACT

The synthesis and photovoltaic study of five dyes based on 4*H*-pyranylidene moiety as donor moiety is reported. A thiophene unit conjugated with/without an ethynyl bond acts as the π-relay and benzoic acid as the anchor group with/without a trifluoromethyl group. Their electrochemical and optical properties are analyzed by using a joint experimental and theoretical approach. The presence of the trifluoromethyl group leads to an enhancement of the molar extinction coefficient, being slightly when a hexyl chain is introduced in the thiophene ring, but does not modify the oxidation potential.

For the preparation of derived solar cells an antiaggregant is essential in all cases. The photovoltaic performance is sensitive to the structural modification of the dye: the CF_3 group and the hexyl chain of the thiophene spacer were shown to improve the efficiency. The lack of a triple bond in the π-spacer involves a lower photovoltaic efficiency, and the trifluoromethyl group leads to a lower dye-load, but a decrease of the recombination processes. These results are in accordance with the electrochemistry impedance spectroscopy studies carried out. Moreover, the organic dyes have been also tested with a fluorescent lamp (indoor conditions), leading to an increase of the efficiency, reaching a 36% for the best dye.

1. Introduction

Dye-sensitized solar cells (DSSCs) have attracted much interest in the search of alternative photovoltaics (PV) technologies based on cost-effective and environmentally friendly materials [1–3]. Over the past two decades a tremendous effort has been made to search for more efficient sensitizers, but the power conversion efficiency values have stagnated at around 14%, generally using a co-sensitization strategy [4–7] and are still low when compared with silicon solar cells, bulk-hetero-junction solar cells (BHJ) and perovskite solar cells (PSC).

Recently there has been a renaissance of DSSC due to its potential as Building-Integrated Photovoltaics (BIPV) taking advantage of the possibility of preparing colored and long-term stable semi-transparent modules [8–10].

DSSCs are also promising in the fields of wearable/portable electronics since they are lightweight, mechanically flexible and can be easily integrated in other devices. A further strength of DSSC consists in their high performance under indoor conditions in comparison to other solar technologies [11–13].

Metal-free organic dyes represent one of the main class of photosensitizers for DSSCs because their chemical structures are tunable by exploiting well-stablish synthetic strategies in the field. The architecture of the most efficient organic sensitizers is based on Donor-π spacer-Acceptor (D-π-A) structures [14,15]. A D-π-A configuration facilitates the photoinduced intramolecular charge-transfer (ICT) from donor to acceptor moieties promoting the electron injection into the conduction band of the semiconductor. A great effort has been devoted to obtain D-π-A systems with tailored optical properties, well-aligned electronic levels, and high stability. The molecular structure of dyes can be modulated to achieve the requirements previously mentioned to get a significant power conversion efficiency (PCE) enhancement in DSSCs. A wide number of donors and π-spacers have been explored, whereas a few molecular groups have been studied as electron acceptor/anchoring moieties [16].

The donor capability of 4*H*-pyranylidene ring has been widely supported due to its proaromatic nature [17]. This fact, together with its synthetic versatility represents a great advantage keeping this unit into focus for a myriad of areas: second nonlinear optics [17–21], organic

* Corresponding author.
** Corresponding author.
E-mail addresses: sfranco@unizar.es (S. Franco), randreu@unizar.es (R. Andreu).

https://doi.org/10.1016/j.dyepig.2022.110566
Received 20 January 2022; Received in revised form 1 June 2022; Accepted 8 July 2022
Available online 19 July 2022

photovoltaics [22], two-photon absorption materials [23], hole-transporting materials for perovskite solar cells [24] or probes for biological imaging [25].

Regarding DSSCs field, the γ-pyranylidene moiety has been successfully evaluated in various series of D-π-A systems [26–31]. The donor properties of this unit are similar, if not higher than the ones observed in triarylamines [32]. Efficiencies above 6% and 7% have been achieved for 4*H*-pyranylidene dyes featuring a thienothiophene core decorated by *n*-hexyl chains as π-spacer [33] or for twisted compounds with an additional thiophene ring in the exocyclic C═C double bond [34].

Among the spacer, the thiophene unit is frequently used as π-conjugated bridge due to its excellent charge-transport properties. A common strategy to avoid dye-aggregation involves the incorporation of bulky groups, like alkyl groups, into the structure of the molecule. The presence of alkyl chains in the structure promotes the hydrophobicity, which contributes to the long-term stability, as well as increases the electron lifetime, responsible of an improvement of the V_{oc} values [35].

The incorporation of triple bonds into a D-π-A dye could red-shift the absorption spectrum and enhance the IPCE curve [36]. Moreover, the presence of an ethynyl linkage in a sensitizer can fine-tune the energy levels of the dyes [37].

Cyanoacrylic and benzoic acid are, by far, the acceptor units the most studied and with the best results obtained. On certain occasions, with the aim of tuning and enhancing the performance and the stability of sensitizers, electron-poor functional groups have been incorporated in the π-spacer with good results [38,39]. In this context, the trifluoromethyl group as substituent of benzoic acid has been rarely explored in DSSCs [40].

In light of the abovementioned, we present the study of four D-π-A dyes (compounds **1a-b**, **2a-b**, Fig. 1) which have been designed according to the following approach: i) the 2,6-diphenyl-4*H*-pyranylidene ring acts as the donor moiety; ii) the thiophene unit conjugated with an ethynyl bond plays the role of the π-relay, with compounds of series **b** having a *n*-hexyl chain, and iii) the benzoic acid is the anchor group with (compounds **2**) or without (compounds **1**) a trifluoromethyl group in order to study the effect of this structural modification on the photovoltaic properties.

An analogous derivative to **2b**, lacking the acetylene bond (compound **3b**, Fig. 1) is also included in the study for the sake of comparison.

The electronic and optical properties of the dyes were accomplished by means of electrochemistry, spectroscopic techniques, and quantum chemical methods. On the other hand, the influence of a *n*-hexyl chain on the thiophene ring has also been studied.

In recent years, there has been again a growing interest in DSSC,

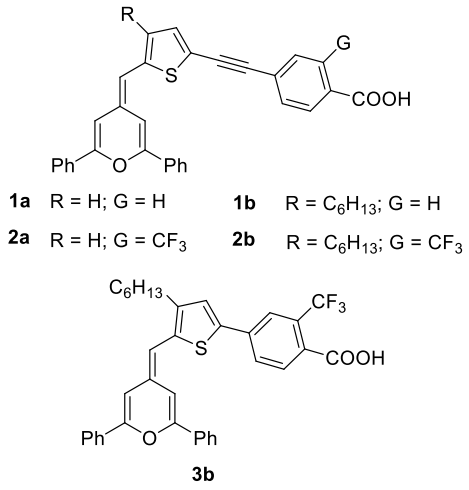

Fig. 1. Molecular structures of the targeted dyes.

mainly due to their good response under ambient light conditions [12,41–43]. Excellent efficiencies have been described by employing electrolytes based on cupper [11,44] and cobalt [45] complexes or in quasi-solid-state [46] at reduced light intensities. For this reason, the organic dyes shown in Fig. 1 have been also tested at intensities lower than 1 sun and with a fluorescent lamp.

2. Results and discussion

2.1. Synthesis

For the synthesis of the final compounds **1a–b** and **2a–b**, the previous preparation of 4*H*-pyranylidene-containing protected alkynes **6a-b** is required.

Compounds **6a–b** were prepared by a Horner reaction between (2,6-diphenyl-4*H*-pyran-4-yl)diphenylphosphine oxide **4** [47] and the corresponding aldehyde **5a–b** [48,49] (Scheme 1). After purification, **6a** was isolated as an orange solid and **6b** as a dark yellow oil.

Next, the synthesis of dye **2a** was accomplished as follows (Scheme 2): first, the deprotection of trimethylsylil group with Bu_4NF in THF took place, obtaining **7a**, which was identified by ^1H NMR (see Fig. S-5) and used directly, without any purification, in a Sonogashira coupling with the benzoic acid derivative **8** [50].

When this method was applied in the synthesis of dyes **1a–b** and **2b**, the purification of final compounds was particularly difficult and tedious. Various purification techniques were unsuccessfully employed (washing with different solvents and centrifugation, column chromatography on silica gel, reversal phase HPLC, among others), obtaining in all cases a minimum amount of the final products.

Hence, a modification to the synthesis showed at Scheme 2 was carried out, using for the Sonogashira reaction the corresponding methyl ester (**9** [51] and **10** [52]) instead of the benzoic acid derivative (Scheme 3). Consequently, a basic hydrolysis of synthesized esters **11a–b** and **12b** was required to afford the final compounds **1a–b** and **2b**, in yields that ranged from 36 to 81%. Yields for Sonogashira step were moderate-low due to the difficult purification of systems **11a-b**, **12b**, particularly for the subsequent repeated chromatographic purification on silica gel (for compounds **11a**, **12b**).

A different approach was adopted for compound **3b**, which was prepared in a three-step synthetic route (Scheme 4). First, a Suzuki coupling [53] between the previously reported aldehyde **13b** [49] and the commercial (4-(methoxycarbonyl)-3-(trifluoromethyl)phenyl) boronic acid **14** resulted in a mixture of esters **15b** + **15b'** (proportion 25/75). Next, a Horner reaction with phosphine oxide **4** afforded compounds **16b** + **16b'** (proportion 25/75). Eventually, the basic hydrolysis of this mixture gave dye **3b**. It is important to note that it was not necessary to separate the intermediate product mixtures since the final hydrolysis produced only the desired product (**3b**). It may be striking to propose a synthesis that results in a mixture of esters, but the use of ethanol instead of methanol improved the overall yield of the process. Nevertheless, although the synthetic process was optimized, a yield of 8% was obtained after the three steps.

2.2. Optical properties

The absorption spectra of the dyes in CH_2Cl_2 and on TiO_2 electrodes are shown in Fig. 2 and the photophysical data are collected in Table 1.

All dyes exhibit a broad absorption band ranging from 350 to 550 nm which can be attributed to the ICT from the proaromatic donor to the carboxylic acid. The energy of the ICT transition does not follow a general rule. A bathochromic effect is observed upon the introduction of a hexyl chain on the thiophene ring, being slightly in the case of **1a** →**1b**.

The presence of the trifluoromethyl group has a different effect depending on the structure of the thienyl spacer, since a hypsochromic or bathochromic effect was observed for series **a** and **b**, respectively.

The introduction of this electron deficient group provides in series **a**

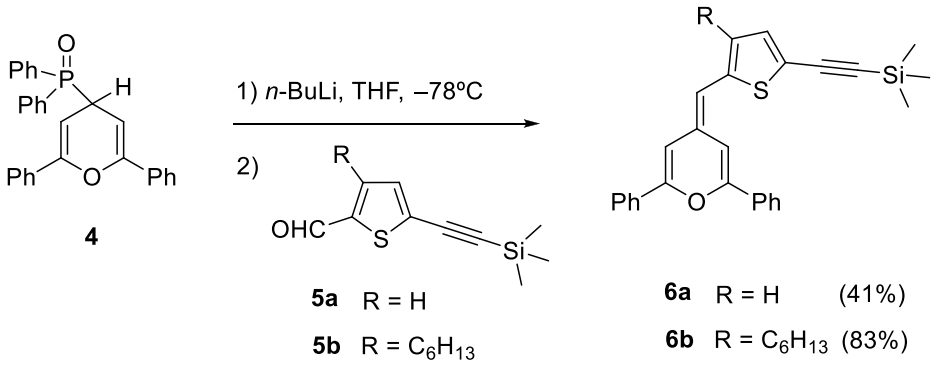

Scheme 1. Synthesis of compounds **6a–b**.

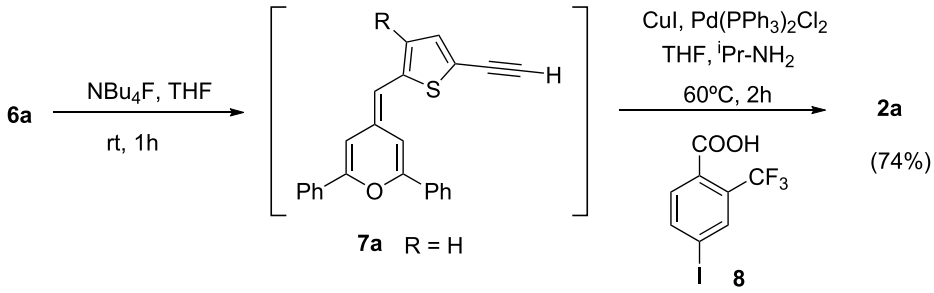

Scheme 2. Synthesis of dye **2a**.

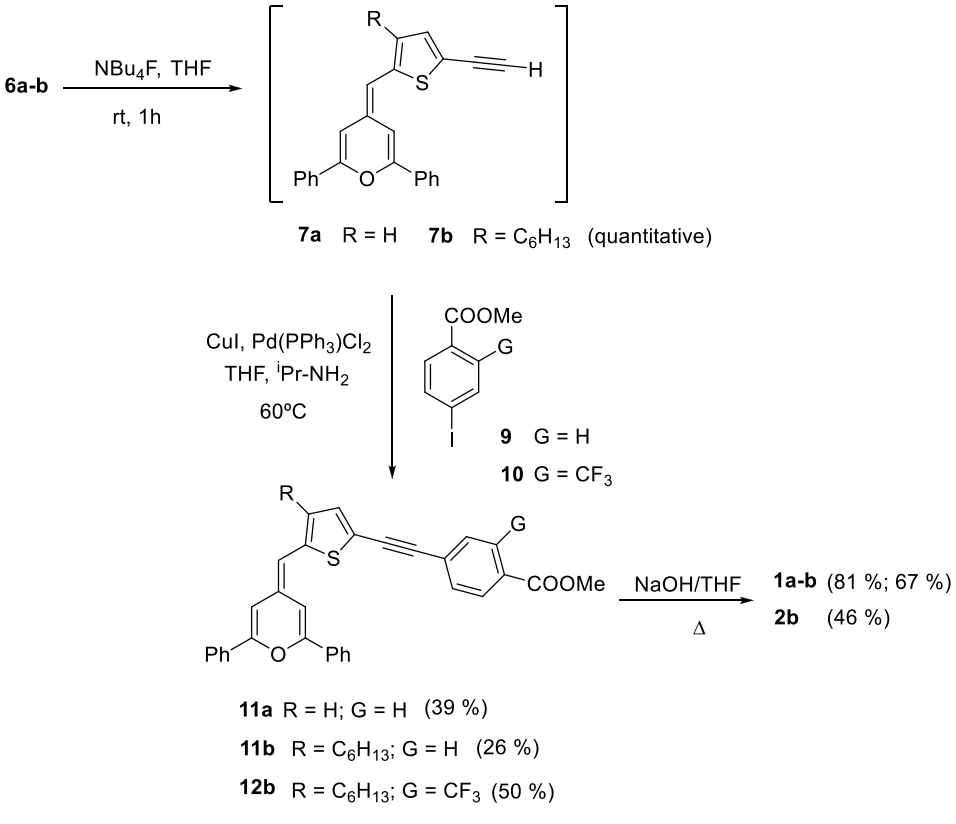

Scheme 3. Synthesis of dyes **1a–b** and **2b**.

(R = H; Fig. 1) an increase of the molar extinction coefficient (ε), which is an essential parameter to ensure a good light energy absorption. Thus, compound **2a** presents the highest value. Concerning series **b** (R = C_6H_{13}; Fig. 1), the variation of ε is slight on passing from **1b** to **2b**. On the other side, it is important to remark that all dyes present ε values exceeding those of the standard ruthenium dyes.

On the other hand, the absence of the triple bond in dye **3b** compared to **2b**, provokes a blue-shift of the absorption, in agreement with the less

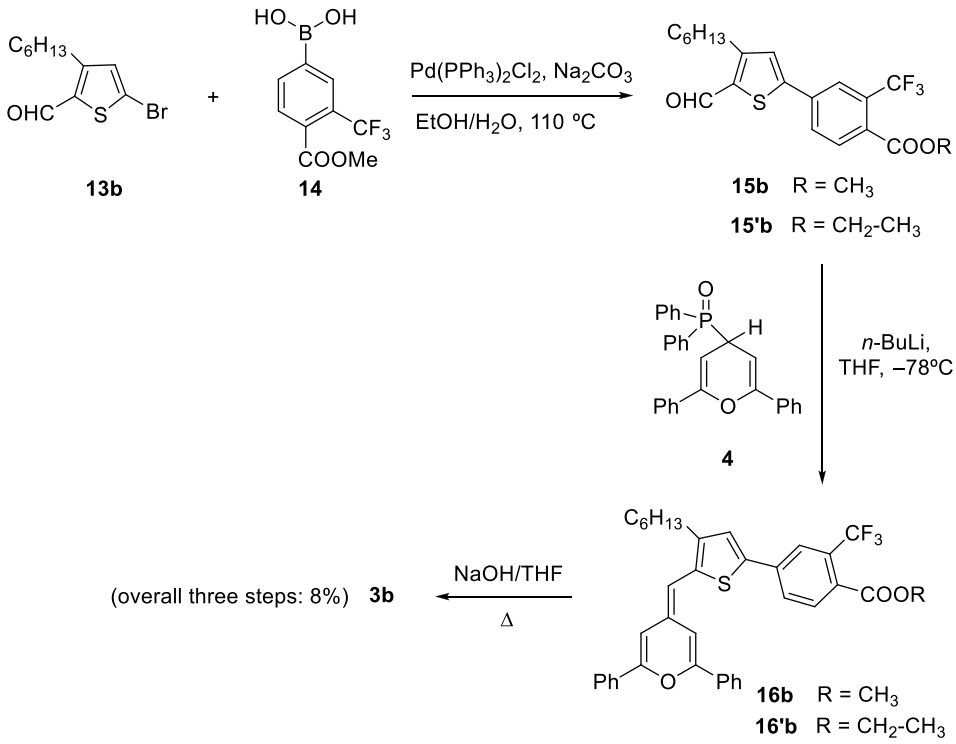

Scheme 4. Synthetic route for dye **3b**.

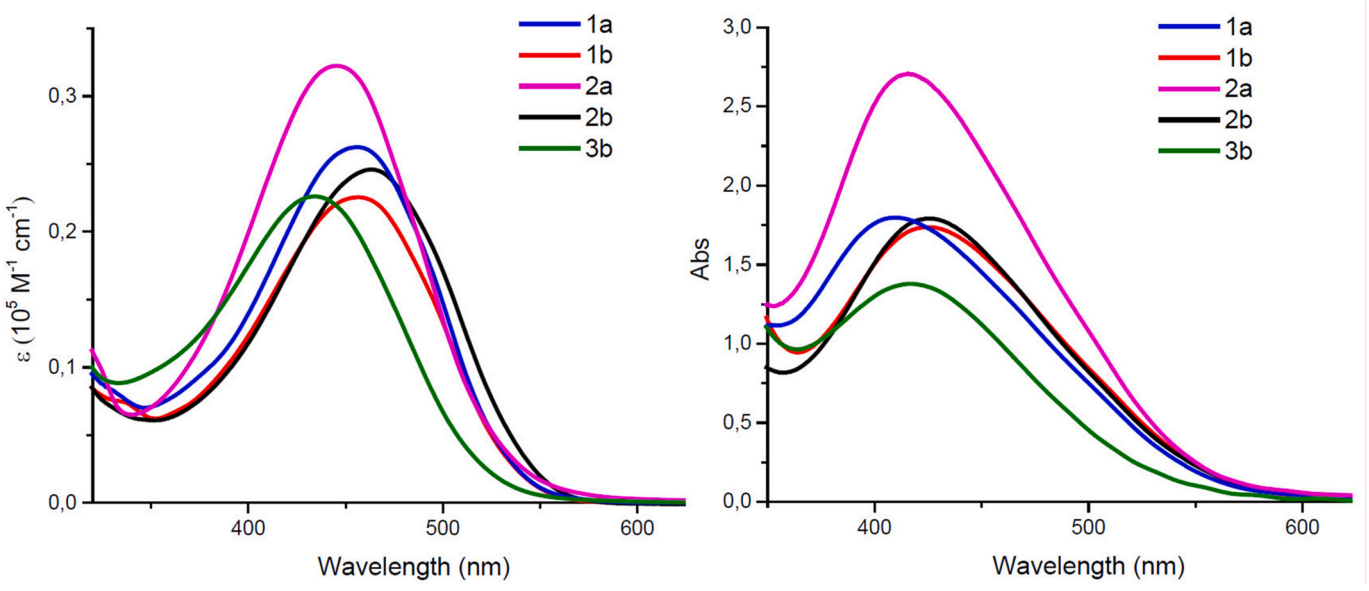

Fig. 2. Absorption spectra of dyes in CH_2Cl_2 (left) and on TiO_2 films (right).

π-extended system, together with a decrease of the ε value. This is in accordance with the study of other D-π-A dyes lacking/containing a C≡C bond in their structure [36,37].

When the dyes are attached to TiO_2 surface, the maximum absorption peaks are blue shifted around 30 nm as compared to those in solution. In general, this hypsochromic shift may be attributed to the deprotonation of the carboxylic acid upon adsorption onto the TiO_2 surface, due to the weaker electron character of the carboxylate-TiO_2 unit [54–56]. (See in the Supporting Information, the measure of absorption of films at different immersion times, Figures S-47−S-51).

2.3. Electrochemical study

The electrochemical properties of the dyes were studied by differential pulse voltammetry (DPV). The ground-state oxidation potential (E_{ox}) of each dye was determined in CH_2Cl_2 (Table 1). The voltammograms (Fig. 3) were performed using 0.1 M tetrabutylammonium hexafluorophosphate as the supporting electrolyte, a glassy carbon working electrode, a Pt counter electrode and Ag/AgCl reference electrode.

The E_{ox} is in all cases higher than the redox potential of the iodide/triiodide couple (+0.4 V *vs* NHE) [57] allowing the regeneration of the oxidized form of the sensitizer. Except for the compound **2a**, no large differences have been observed in the measured oxidation potentials,

Table 1
Optical properties and electrochemical data.

Dye	λ_{abs}, nm (ε, M^{-1} cm^{-1})[a]	λ_{abs}, nm[b]	E_{ox},[c] V (vs NHE)	$E_{0\text{-}0}$,[d] eV	E^*_{ox},[e] V (vs NHE)
1a	455 (26260 ± 810)	410	+0.91	2.32	−1.41
1b	457 (22330 ± 730)	425	+0.88	2.31	−1.43
2a	444 (34400 ± 1300)	415	+0.98	2.34	−1.36
2b	462 (23550 ± 460)	426	+0.91	2.27	−1.36
3b	434 (22990 ± 360)	416	+0.92	2.38	−1.46

[a] Absorption maxima in CH_2Cl_2 solution.
[b] Absorption maxima on TiO_2 films (4 μm thick).
[c] First oxidation potentials measured in CH_2Cl_2 with 0.1 M $TBAPF_6$ as electrolyte, Ag/AgCl as reference electrode and Pt as counter electrode respectively. Potentials were converted to normal electrode (NHE) by addition of 0.199 V.
[d] Zeroth-zeroth transition energies estimated from the absorption spectrum, that is calculated drawing the tangent to the curve (λ_{max}) on the side of lower energy. The Planck-Einstein formula, $E = hc/\lambda$ is applied.
[e] Excited-state oxidation potential obtained from $E_{ox} - E_{0\text{-}0}$.

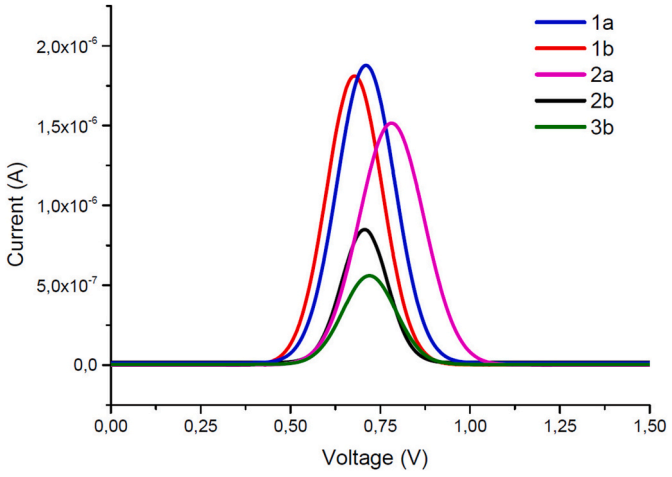

Fig. 3. Differential pulse voltammetry (DPV) in CH_2Cl_2 solution for synthesized dyes.

indicating that the presence of the trifluoromethyl group or the hexyl chain in the thiophene ring hardly affect the oxidation of the donor moiety.

The excited-state oxidation potentials (E^*_{ox}) were obtained from the expression E_{ox}–$E_{0\text{-}0}$, with the band gap energies ($E_{0\text{-}0}$) estimated from the absorption spectra (Table 1). For all the cases, E^*_{ox} value is more negative than the conduction band edge of TiO_2 (−0.5 V *vs* NHE) [58] allowing an effective electron injection from the excited sensitizers to the semiconductor conduction band.

2.4. Theoretical calculations

Density Functional Theory (DFT) calculations provide a complementary theoretical study to obtain further information of the optical and electrochemical behavior of the synthesized dyes. The CPCM (Conductor-like Polarizable Continuum Model) solvation method has been performed. The most relevant parameters deduced from the calculations are summarized in Table 2.

Calculated absorption wavelengths are overestimated for all dyes by 14–49 nm, but the data are in reasonable agreement with the experimental results. The experimental trends discussed in the optical properties section (2.2) are well reproduced except for the hypsochromic

Table 2
Results of DFT calculations at the CPCM-M06-2x/6–311 + G(2d,p)//M06-2x/6-31G* level in CH_2Cl_2.

Dye	λ_{abs}[a] (nm)	E_{HOMO} (eV)	E_{LUMO} (eV)	λ_{em}[a] (nm)	$E_{0\text{-}0}$ (eV)	E_{ox}[b] (V)	E^*_{ox}[b,c] (V)
1a	469	−6.21	−1.79	625	2.26	+0.77	−1.49
1b	480	−6.13	−1.77	648	2.22	+0.71	−1.51
2a	477	−6.24	−1.92	638	2.21	+0.84	−1.36
2b	490	−6.16	−1.91	663	2.14	+0.70	−1.44
3b	483	−6.17	−1.80	662	2.14	+0.70	−1.44

[a] Calculated using equilibrium solvation.
[b] Referenced to NHE.
[c] The oxidation potential of the excited state of the dye was calculated from $E^*_{ox} = E_{ox} - E_{0\text{-}0}$.

effect due to the incorporation of the CF_3 substituent when comparing compounds **1a** and **2a**.

Likewise, theoretical oxidation potential values are underestimated but correlate well with the experimental data.

Concerning the electron densities related to frontier orbitals (See Fig. 4 for compound **2a** and Supporting Information for the rest) the HOMO is mainly supported by the 4*H*-pyranylidene unit and the thienyl ring, while the ethynylbenzoic acid fragment contributes most for the LUMO. The energy absorption between the ground state to the first excited state involves an ICT mainly contributed by a one electron promotion from the HOMO to the LUMO. Both frontier orbitals spread along the whole D-π-A system leading to a large HOMO-LUMO overlap that can explain the high ε values observed.

Regarding the geometrical configuration in the ground state, the π−system for all dyes is almost planar except for compound **3b**, lacking the triple bond connecting the thiophene ring and the acceptor moiety. This structural feature gives rise in compound **3b** to a rotation between the thiophene unit and the benzoic acid with a dihedral angle of 15° (See Fig. S-39). This geometric arrangement implicates a less efficient conjugation that is in accordance with the hypsochromic shift observed on passing from **2b** to **3b** (see Table 1) and it allows to explain the very low value of efficiency obtained (see photovoltaic properties, section 2.5).

The presence of an alkyl group does not alter the planar configuration between the 4*H*-pyranylidene and the thienyl unit in compounds **1b**, **2b** and **3b**, which guarantees the transfer of electrons from the donor to the acceptor group, incorporating a bulky group than can prevent the aggregation.

Considering the spin plots calculated for the oxidized radical cations for all dyes, it should be noted that most of the spin density spreads (Fig. 5 for compound **2a** and Supporting Information for the rest) on the 4*H*-pyranylidene donor and the thiophene spacer, making difficult the undesirable back electron transfer (BET) from the TiO_2 electrode.

2.5. Photovoltaic properties

The photovoltaic properties of the sensitizers were evaluated under standard AM 1.5 G illumination (100 mW cm^{-2}) using a solar simulator (See Supporting Information). The solar cells were fabricated following a protocol that we have already described in previous papers. In this series, the optimized concentration was defined as 0.1 mM for the sensitizer and 0.3 mM for the antiaggregant additive chenodeoxycholic acid in anhydrous CH_2Cl_2. (Mixtures EtOH/CH_2Cl_2 (1:1) and increased concentrations of antiaggregant were also tested, although there is not improvement in the results). The liquid electrolyte was based on the redox I^-/I_3^- system (1-butyl-3-methylimidazolium iodide (0.53 M), LiI (0.10 M), I_2 (0.050 M) and *tert*-butylpyridine (0.52 M) in anhydrous acetonitrile). The photoanodes were prepared using the screen-printing technique with a commercial TiO_2 paste (Dyesol® 18NR-AO) and an effective area of 0.25 cm^2. The thickness of active layer was optimized to 13 μm and the dipping time was set to 8 h.

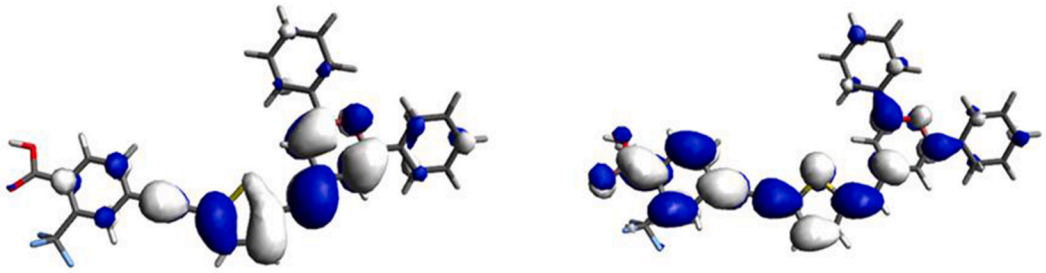

Fig. 4. Illustration of the HOMO (left) and LUMO (right) of compound **2a**.

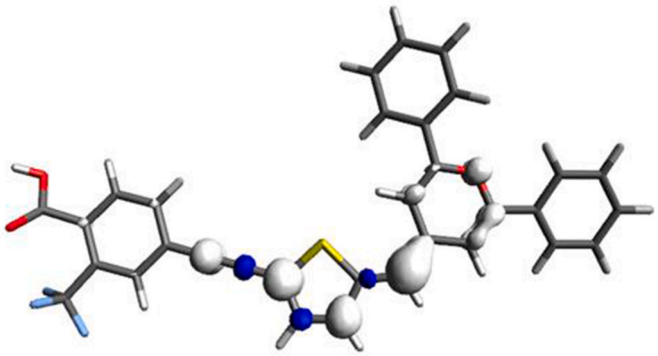

Fig. 5. Spin density plot of radical cation of compound **2a**.

The photocurrent-voltage (J/V) curves of all dyes were measured either under AM1.5G at different intensities (100 mW/cm^2 (1 sun), 77 mW/cm^2), and under indoor light using a fluorescent lamp (OSRAM 930/18W) at 2000 lux (0.708 mW/cm^2) and 1000 lux (0.350 mW/m^2).

Table 3 shows a summary of the significant photovoltaic parameters determined from the photovoltaic measurements, from which the performance of the solar devices is evaluated. The current density-voltage (*J-V*) curves and incident photon-to- current conversion efficiencies (IPCE) at 1 sun are depicted in Fig. 6. (See Fig. S-53 for data at 2000 lux and 1000 lux).

The DSSC based on dye **2b** achieved the highest PCE of series (4.13%) with a J_{sc} of 10.67 mA/cm^2, V_{oc} of 595 mV, and *ff* of 65.0%. A significant reduction in PCE has been observed in the absence of anti-aggregant, which may indicate that the compounds in this series have a great tendency to form aggregates, due to the high degree of planarity of the molecules. In any case, the increase in V_{oc} values for dyes **1b** and **2b** are, probably due to the incorporation of the hexyl group which inhibits the intermolecular π-π aggregation. PCE for compound **3b** drops to 2.68% mainly due to a lower J_{sc} value than compounds **1b**, **2b** which indicates that the absence of the acetylenic bond significantly reduces the electron transfer throughout the molecule, resulting in an inefficient injection to the TiO_2 electrode. The low efficiency could be explained by a no planar arrangement to the donor and acceptor groups, as shown in the theoretical calculations section (2.4).

In any case, it can be highlighted that the incorporation of a CF_3 group in the benzene group (**2a**, **2b**) improves the efficiency compared to dyes lacking this structural modification (**1a**, **1b**). The effect is somewhat greater for the series **a**, without the hexyl group. In order to find a possible explanation, a study has been carried out to determine the amount of dye adsorbed on the titanium electrode. Table 3 summarizes data obtained and it can be stated that the presence of a CF_3 group leads to a lower dye loading, while the V_{oc} values increase, explaining the observed efficiencies.

The dyes were also measured in lower light conditions (77 mW/cm^2) observing, in all cases, practically identical PCE values (Table 3). The efficiency values improved substantially when the measurements were

Table 3
Photovoltaic parameters[a]: the open circuit voltage (V_{oc}), the short circuit current (J_{sc}), the fill factor (*ff*), solar-to-electrical energy conversion efficiency (η) and electron lifetimes (τ_n).

Dye	Irradiance (mW/cm^2)	Illuminance [c] (lux)	V_{oc} (mV)	J_{sc} (mA/cm^2)	*Ff* (%)	PCE (%)	τ_n (ms)	Dye-load (mol/cm^2)
1a	100[b]	–	510	9.50	61.0	2.96	3.68	9.44×10^{-8}
	77 [b]	–	503	7.16	63.0	2.99		
	0.350	1000	390	0.0482	69.6	3.74		
	0.708	2000	395	0.0940	68.6	3.59		
1b	100 [b]	–	565	10.94	64.3	3.98	6.70	1.01×10^{-7}
	77 [b]	–	551	8.36	66.3	3.97		
	0.350	1000	428	0.0543	71.2	4.73		
	0.708	2000	442	0.1095	71.3	4.81		
2a	100 [b]	–	533	9.84	65.2	3.42	4.96	6.61×10^{-8}
	77 [b]	–	528	7.507	67.0	3.45		
	0.350	1000	415	0.0451	73.6	3.93		
	0.708	2000	425	0.0886	72.5	3.86		
2b	100 [b]	–	595	10.67	65.0	4.13	7.61	8.72×10^{-8}
	77 [b]	–	589	8.21	66.1	4.15		
	0.350	1000	445	0.0597	74.4	5.64		
	0.708	2000	450	0.1167	75.0	5.56		
3b	100 [b]	–	541	7.30	67.9	2.68	6.42	3.24×10^{-8}
	77 [b]	–	537	5.74	68.2	2.73		
	0.350	1000	400	0.0375	71.5	3.07		
	0.708	2000	429	0.0720	71.9	3.18		

[a] Data obtained in all cases with devices of 0.25 cm^2 working area and 13 mm thick in presence of chenodeoxycholic acid (0.3 mM) in CH_2Cl_2.
[b] Data obtained under simulated AM1.5G solar light at different intensities (100 mW/cm^2 and 77 W/cm^2).
[c] Data obtained with a fluorescent lamp OSRAM 930/18W at 1000 lux and 2000 lux. The lamp spectrum is illustrated in the ESI, Fig. S-52. The stabilized illumination intensity was calibrated with a commercial photo/radiometer Delta Ohm HD2102.1 and a LP 471 phot probe.

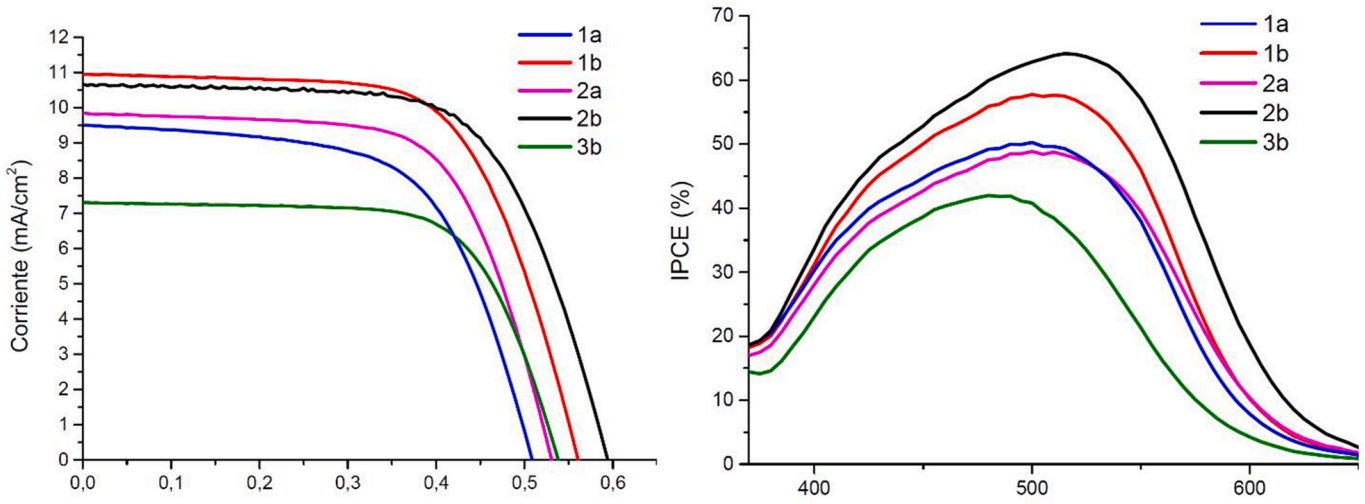

Fig. 6. Current density-voltage curves (left) and IPCE spectra (right) of the DSSC based on dyes **1a-b**, **2a-b**, **3b**.

carried out with the fluorescent lamp. In most cases, the highest values were obtained at 1000 lux and it is worth highlighting the compound **2b** with an increase of 36% (5.64% *vs* 4.13%). These results are not surprising because the absorption UV–vis curves of the dyes overlap better with the fluorescent light emission wavelength (See Fig. S-52).

IPCE spectra are shown in Fig. 6 and it can be observed that the wavelength response range of the sensitizers is about 355–700 nm and are consistent with their absorption properties. The highest J_{sc} value measured for **2b** agrees with their most intense and broadest IPCE curve, that exceeds 60% from 500 to 560 nm.

The lowest maximum of 42% for compound **3b** indicates that the injection of electrons is less favored. This is in agreement with a low J_{sc} value and the lowest dye load on the electrode.

2.6. EIS experiments

Electrochemistry impedance spectroscopy (EIS) [59,60] is an electrochemical technique that allows the analysis of electron transport kinetics in DSSC and gives an idea of the recombination of charges, which in turn can be correlated with the V_{oc} values. The measurements were carried out under AM 1.5G simulated solar light (100 mW cm^{-2}) at open circuit voltage conditions. (Fig. 7). The electron lifetimes (τ) were estimated from the Bode plots following the equation $\tau = 1/2\pi f$ (where f = frequency at the maximum of the curve). The interfacial charge recombination resistances can be estimated fitting the EIS spectrum with the equivalent circuit model (Fig. 7) when R is the total resistance of the circuit, R_{tr} is the transport resistance at the Pt/electrolyte interface (small semicircles) and R_{rec} represents the electron recombination

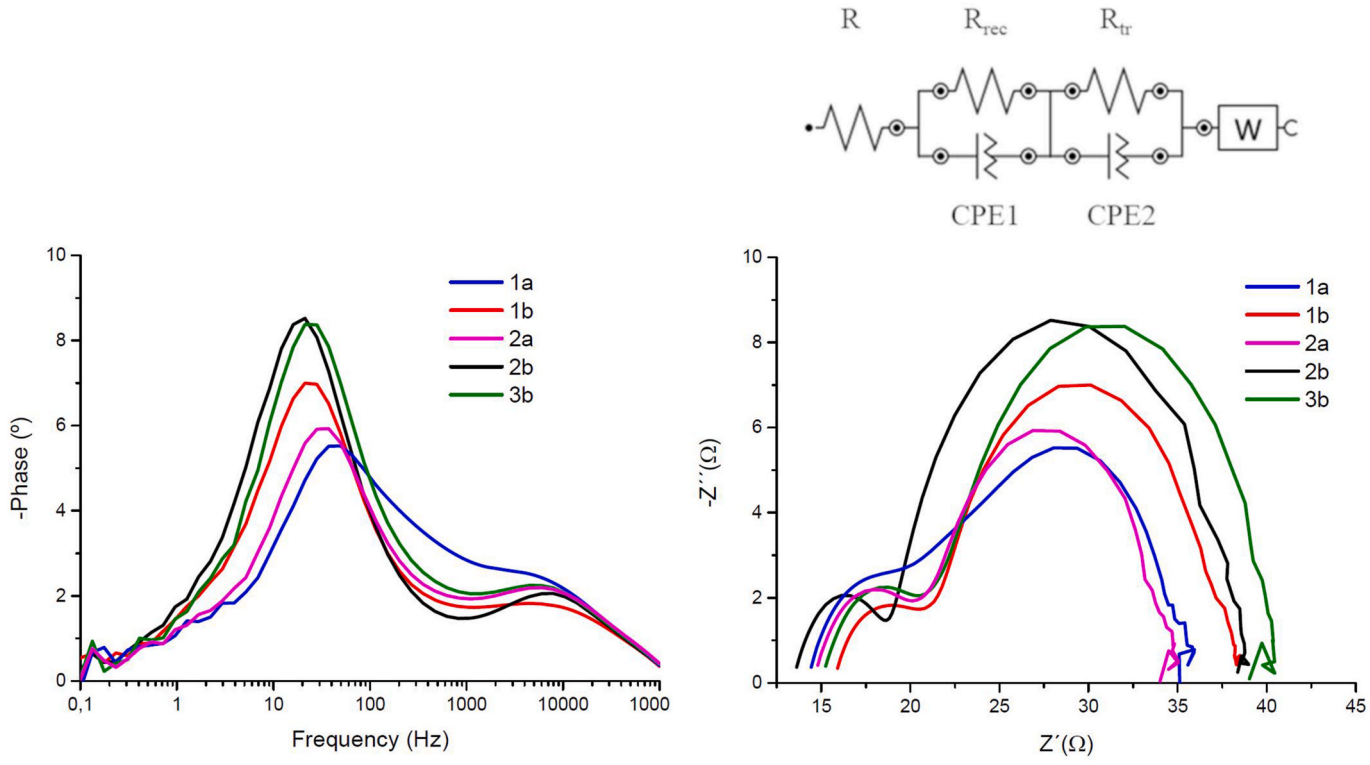

Fig. 7. Nyquist plot (left) and Bode plot (right) for DSSCs based on studied dyes.

resistance on the TiO_2/dye/electrolyte interface (big semicircles), CPE1 and CPE2 are constant phase elements that indicate the capacitance of the interface and W is a Warburg element related to the diffusion of I_3^- in the electrolyte.

The obtained values of R_{rec} decreased in the order: **2b** (20.0 Ω) > **1b** (18.2 Ω) > **3b** (17.9 Ω) > **2a** (14.0 Ω) > **1a** (12.9 Ω) and correspond to the trend observed for V_{oc} (a higher recombination resistance usually corresponds to a higher value of V_{oc}). These results seem to indicate that the alkyl substituent and the CF_3 group reduce the recombination processes and are in agreement with the electron lifetimes estimated (Table 3).

The charge-collection efficiencies [61] (η_{cc}) can be estimated from the EIS parameters applying the formula $\eta_{cc} = R_{rec}/(R_{rec} + R_{tr})$. The found values are for **1a** (0.62), **1b** (0.79), **2a** (0.70), **2b** (0.81) and **3b** (0.72), which show that devices based on dye **2b** inject electrons more efficiently, thus obtaining higher V_{oc} values.

3. Experimental

3.1. General experimental methods

See Supporting Information.

3.2. Device preparation and characterization

See Supporting Information.

3.3. Computational details

See Supporting Information.

3.4. Starting materials

Compounds **4** [47], **5a–b** [48,49], **8** [50], **9** **[51]** and **13b** [49] were prepared as previously described.

Boronic acid **14** is commercially available.

3.5. Synthesis and characterizations

3.5.1. ((5-((2,6-diphenyl-4H-pyran-4-ylidene)methyl)thiophen-2-yl) ethynyl)trimethylsilane (6a)

A solution of (2,6-diphenyl-4*H*-pyran-4-yl)diphenylphosphine oxide (**4**) (1.67 g, 3.84 mmol) in 20 mL of anhydrous THF was prepared under argon and cooled to −78 °C. To this solution, *n*-BuLi 1.6 M in hexanes (2.77 mL, 4.43 mmol) was added dropwise and the resulting mixture was stirred at −78 °C for 20 min. Then, a solution of aldehyde **5a** (800 mg, 3.84 mmol) in 10 mL of anhydrous THF was added dropwise, the mixture was warmed up to room temperature and stirred overnight. The reaction was quenched by the addition of aqueous saturated NH_4Cl solution, extracted with AcOEt and washed with water (2 × 20 mL). The organic phase was dried over $MgSO_4$ and the solvent was removed under reduced pressure. The crude product was filtered through a layer of silica gel with hexane, and the resulting solid was washed with cool heptane. An orange solid (670 mg, 41%) was finally obtained.

Mp (°C): 97–99. IR (KBr): ῡ (cm^{-1}) = 3064 (Csp^2–H), 2957 (Csp^3–H), 2138 (C≡C), 1656 and 1577 (C═C, Ar), 1246 (Si–C). ^{1}H NMR (400 MHz, acetone-d_6): δ (ppm) 7.90–7.87 (m, 2H), 7.83–7.80 (m, 2H), 7.58–7.44 (m, 4H), 7.20 (d, J = 3.9 Hz, 1H), 7.11 (dd, J_1 = 2.0 Hz, J_2 = 0.7 Hz, 1H), 6.93 (dd, J_1 = 3.9 Hz, J_2 = 0.7 Hz, 1H), 6.72 (d, J = 2.0 Hz, 1H), 6.19 (s, 1H), 0.26 (s, 9H). ^{13}C NMR (100 MHz, acetone-d_6): δ (ppm) 154.8, 152.0, 144.8, 134.2, 133.8, 133.7, 130.8, 130.3, 129.8, 129.8, 129.7, 126.4, 126.0, 125.4, 120.1, 109.2, 108.5, 103.0, 100.1, 99.3, 0.0. HRMS (ESI^+) *m/z*: 425.1379 $[M+H]^+$; calculated for $C_{27}H_{25}OSSi$: 425.1390.

3.5.2. ((5-((2,6-diphenyl-4H-pyran-4-ylidene)methyl)-4-hexylthiophen-2-yl)ethynyl)trimethylsilane (6b)

A solution of (2,6-diphenyl-4*H*-pyran-4-yl)diphenylphosphine oxide (**4**) (1.48 g, 3.42 mmol) in anhydrous THF (30 mL) was prepared under argon and stirred at −78 °C, then n-BuLi 1.6 M in hexanes (2.32 mL, 3.83 mmol) was added dropwise. After 20 min, a solution of the aldehyde **5b** (1g, 3.42 mmol) in anhydrous THF (7 mL) was added and the reaction was warmed up to room temperature overnight. A saturated solution of NH_4Cl (30 mL) was added and the product was extracted with AcOEt (3 × 20 mL). The organic layer was washed with water (2 × 30 mL), dried over $MgSO_4$ and evaporated. The crude product was filtered through a layer of silica gel with hexane, affording compound **6b** as a dark yellow oil (1.44 g, 83%).

^{1}H NMR (300 MHz, acetone-d_6): δ (ppm) 7.99–7.88 (m, 4H), 7.60–7.42 (m, 6H), 7.12 (dd, J_1 = 1.9 Hz, J_2 = 0.6 Hz, 1H), 6.88 (s, 1H), 6.75 (d, J = 1.9 Hz, 1H), 6.18 (s, 1H), 2.72–2.60 (m, 2H), 1.72–1.54 (m, 2H), 1.41–1.23 (m, 6H), 0.92–0.82 (m, 3H), 0.26 (s, 9H). ^{13}C NMR (100 MHz, acetone-d_6): δ (ppm) 154.6, 150.1, 143.0, 133.8, 133.7, 130.8, 130.2, 129.9, 129.7, 129.6 (× 2), 127.7, 125.9, 125.3, 109.2, 108.7, 103.1, 102.4, 99.1, 98.6, 32.3, 30.7, 29.9, 29.6, 23.3, 14.4, 0.1. MS (MALDI) *m/z* 508.2 $[M^{+\cdot}]$.

3.5.3. 4-((5-ethynylthiophen-2-yl)methylene)-2,6-diphenyl-4H-pyran (7a)

To a solution of **6a** (115 mg, 0.3 mmol) in anhydrous THF (5 mL) was added dropwise NBu_4F 1 M in THF (0.27 mL, 0.3 mmol) under argon. After stirring 40 min at room temperature the reaction was quenched by the addition of water. The product was extracted with AcOEt (2 × 20 mL) and the organic layer was dried over anhydrous $MgSO_4$. After the removal of the solvent and volatile compounds, a waxy orange solid was obtained and identified by ^{1}H NMR (96 mg, 0.3 mmol). It is used without any purification.

^{1}H NMR (300 MHz, acetone-d_6): δ (ppm) 8.03–7.94 (m, 2H), 7.92–7.88 (m, 2H), 7.67–7.38 (m, 6H), 7.24 (d, J = 3.9 Hz, 1H), 7.16 (dd, J_1 = 2.0 Hz, J_2 = 0.8 Hz, 1H), 6.97 (dd, J_1 = 3.9 Hz, J_2 = 0.8 Hz, 1H), 6.77 (dd, J_1 = 2.0 Hz, J_2 = 0.4 Hz, 1H), 6.23 (s, 1H), 4.09 (s, 1H).

3.5.4. 4-((5-ethynyl-3-hexylthiophen-2-yl)methylene)-2,6-diphenyl-4H-pyran (7b)

This compound was prepared by following the same procedure as for **7a**, starting from 0.3 mmol of compound **6b**. A dark brown oil was obtained and identified by ^{1}H NMR. This compound is directly used for the following synthesis without any purification (130 mg, 0.3 mmol).

^{1}H NMR (300 MHz, acetone-d_6): δ (ppm) 8.04–7.81 (m, 4H), 7.61–7.42 (m, 6H), 7.14 (dd, J_1 = 2.0 Hz, J_2 = 0.7 Hz, 1H), 6.89 (s, 1H), 6.75 (dd, J_1 = 2.0 Hz, J_2 = 0.4 Hz, 1H), 6.18 (s, 1H), 4.18 (s, 1H), 2.73–2.63 (m, 2H), 1.70–1.59 (m, 2H), 1.41–1.28 (m, 6H), 0.93–0.85 (m, 3H).

3.5.5. Methyl 4-iodo-3-(trifluoromethyl)benzoate (10)

To a solution of acid **8** (500 mg, 1.58 mmol) in 10 mL of freshly distilled methanol concentrated sulfuric acid (0.33 mL) was added. The mixture was heated at 70 °C under argon atmosphere for 42 h, then, the solution was allowed to cool to room temperature. It was diluted with water and then, extracted with AcOEt (2 × 10 mL). The organic layer was dried over $MgSO_4$ and the solvent was removed under reduced pressure. The crude was purified by centrifugal thin-layer chromatography on silica gel with hexane/AcOEt (9:1) as eluent, obtaining **10** as a colorless oil (297 mg, 57%).

^{1}H NMR (400 MHz, $CDCl_3$): δ (ppm) 8.08–8.07 (m, 1H), 7.96 (ddd, J_1 = 8.1 Hz, J_2 = 1.8 Hz, J_3 = 0.6 Hz, 1H), 7.51 (dd, J_1 = 8.1 Hz, J_2 = 0.8 Hz, 1H), 3.92 (s, 3H). ^{13}C NMR (100 MHz, $CDCl_3$) δ (ppm) 166.5, 141.0, 135. 8 (q, J = 5.7 Hz), 131.8, 130.3 (q, J = 33.2 Hz), 130.4, 122.2 (q, J = 274.2 Hz), 97.4, 53.0. ^{19}F NMR (376 MHz, $CDCl_3$) δ (ppm) −59.9.

3.5.6. 4-((5-((2,6-diphenyl-4H-pyran-4-ylidene)methyl)thiophen-2-yl) ethynyl)-2-(trifluoromethyl)benzoic acid (2a)

To a solution of **7a** (96 mg, 0.3 mmol), **8** (82 mg, 0.3 mmol), CuI (3 mg, 0.01 mmol) and $Pd(PPh_3)_2Cl_2$ (9 mg, 0.01 mmol) in anhydrous THF (5 mL), diisopropylamine was added dropwise (5 mL, 0.1 mmol) under argon. After stirring 2 h at 60 °C, the reaction was cooled to room temperature and the solvent was removed under reduced pressure. The solid obtained was dissolved in AcOEt, acidified with HCl 2.5 M (2 × 10 mL) and washed with water (2 × 10 mL). The organic phase was dried over anhydrous $MgSO_4$ and the solid obtained from the removal of the solvent was purified by washing with hexane (3 × 15 mL), then with hexane/CH_2Cl_2 (9:1; 3 × 15 mL). Compound **2a** was obtained by centrifugation (40,000 rpm) as a maroon solid (103 mg, 74%).

Mp (°C): 343–345. IR (KBr): ῡ (cm^{-1}) = 3461 (O–H, broad), 3049 (Csp^2–H), 2186 (C≡C), 1704 (C═O), 1645 and 1611 (C═C, Ar), 1163 (C–F). ^{1}H NMR (300 MHz, acetone-d_6): δ (ppm) 8.01–7.86 (m, 6H), 7.63–7.44 (m, 7H), 7.38 (d, J = 3.9 Hz, 1H), 7.18 (d, J_1 = 1.9 Hz, J_2 = 0.5 Hz, 1H), 7.05 (dd, J_1 = 3.9 Hz, J_2 = 0.5 Hz, 1H), 6.80 (d, J = 1.9 Hz, 1H), 6.28 (s, 1H). ^{19}F NMR (376 MHz, acetone-d_6): δ (ppm) −61.4. ^{13}C NMR (75 MHz, THF-d_8): δ (ppm) 167.3, 155.2, 152.5, 146.5, 134.8, 134.7, 134.1, 134.0, 132.1, 130.8, 130.5, 130.2, 129.9, 129.8, 129.7, 127.5, 126.7, 126.2, 126.1, 125.5, 122.6, 119.1, 109.4, 108.5, 103.3, 93.2, 88.2. HRMS (ESI^-) *m/z*: 539.0904 [M − H]$^-$; calculated for $C_{32}H_{18}F_3O_3S$: 539.0934; 495.1016 [M-COOH]$^-$; calculated for $C_{31}H_{17}F_3OS$: 495.1030.

3.5.7. Methyl 4-((5-((2,6-diphenyl-4H-pyran-4-ylidene)methyl)thiophen-2-yl)ethynyl)benzoate (11a)

To a deoxygenated solution of **7a** (331.3 mg, 0.94 mmol), **9** (221.7 mg, 0.85 mmol), CuI (9 mg, 0.047 mmol) and $Pd(PPh_3)_2Cl_2$ (33 mg, 0.047 mmol) in anhydrous THF (18 mL) freshly distilled diisopropylamine (18 mL) was added dropwise under argon. After stirring 5 h at 60 °C, the reaction was cooled to room temperature and the solvent was remove under vacuum. The crude product was filtered through a layer of silica gel with hexane/CH_2Cl_2 (1:1) as eluent and then, it was purified by centrifugal thin-layer chromatography on silica gel using hexane/CH_2Cl_2 (6:4) to provide **11a** as a red oil (197.8 mg, 39%).

Mp (°C): 181–182. IR (KBr): ῡ (cm^{-1}) = 2182 (C≡C), 1721 (C═O), 1654 (C═C), 1601, 1581 and 1558 (C═C, Ar). ^{1}H NMR (400 MHz, CD_2Cl_2) δ (ppm) 8.03–8.00 (m, 2H), 7.91–7.87 (m, 2H), 7.81–7.77 (m, 2H), 7.60–7.57 (m, 2H), 7.54–7.40 (m, 6H), 7.25 (d, J = 3.9 Hz, 1H), 7.15 (dd, J_1 = 2.0 Hz, J_2 = 0.8 Hz, 1H), 6.89 (dd, J_1 = 3.9 Hz, J_2 = 0.8 Hz, 1H), 6.49 (dd, J_1 = 2.0 Hz J_2 = 0.6 Hz, 1H), 6.13–6.12 (m, 1H), 3.91 (s, 3H). ^{13}C NMR (100 MHz, CD_2Cl_2) δ (ppm) 166.9, 154.5, 152.0, 145.5, 133.7, 133.6, 133.4, 131.5, 130.3, 130.1, 130.0, 129.9, 129.8, 129.3, 129.3, 128.4, 126.1, 125.6, 125.1, 119.2, 108.9, 107.8, 103.1, 94.1, 87.3, 52.7. MS (MALDI) *m/z* 486.10 [$M^{+\cdot}$].

3.5.8. 4-((5-((2,6-diphenyl-4H-pyran-4-ylidene)methyl)thiophen-2-yl) ethynyl)benzoic acid (1a)

To a solution of ester **11a** (80 mg, 0.16 mmol) in anhydrous THF (3 mL), an aqueous solution of NaOH (25.6 mg, 4 equiv) was added dropwise and the reaction was stirred under argon at 70 °C for 2 h. The solvent was removed under reduced pressure, and the reaction was acidified to pH 2–3 with 10 mL of 1 M HCl. A red precipitate appears. The solid was filtered and washed with H_2O/EtOH (9:1) (61 mg, 81%).

Mp (°C): 209–211. IR (KBr): ῡ (cm^{-1}) = 3469 (O–H), 2184 (C≡C), 1681 (C═O), 1653 (C═C), 1604, 1579 and 1555 (C═C, Ar). ^{1}H NMR (400 MHz, THF-d_8) δ (ppm) 8.03–8.00 (m, 2H), 7.93–7.90 (m, 2H), 7.86–7.83 (m, 2H), 7.58–7.55 (m, 2H), 7.51–7.40 (m, 6H), 7.25 (d, J = 3.8 Hz, 1H), 7.17 (dd, J_1 = 2.0 Hz, J_2 = 0.8 Hz, 1H), 6.93 (dd, J_1 = 3.9 Hz, J_2 = 0.8 Hz, 1H), 6.67 (d, J = 2.0 Hz, 1H), 6.18 (s, 1H). ^{13}C NMR (100 MHz, THF-d_8) δ (ppm) 167.2, 155.1, 152.5, 146.0, 134.3, 134.2, 134.0, 131.8, 131.6, 130.7, 130.4, 130.2, 129.8, 129.6, 128.6, 126.5, 126.1, 125.5, 120.1, 109.4, 108.6, 103.5, 94.5, 87.2. HRMS (ESI^-) *m/z* 471.0979 [M − H]$^-$; calculated for $C_{31}H_{19}O_3S$: 471.1049.

3.5.9. Methyl 4-((5-((2,6-diphenyl-4H-pyran-4-ylidene)methyl)-4-hexylthiophen-2-yl)ethynyl)benzoate (11b)

To a deoxygenated solution of **7b** (400 mg, 0.92 mmol), **9** (241 mg, 0.92 mmol), CuI (11.68 mg, 0.061 mmol) and $Pd(PPh_3)_2Cl_2$ (42.82 mg, 0.061 mmol) in anhydrous THF (16 mL) freshly distilled diisopropylamine (16 mL) was added dropwise under argon. After stirring 1 h at 60 °C, the reaction was cooled to room temperature and the solvent was removed under vacuum. The crude product was purified by column chromatography on silica gel using CH_2Cl_2/hexane (1:1) as eluent to afford **11b** as a red solid (134 mg, 26%).

Mp (°C): 89–103. IR (KBr): ῡ (cm^{-1}) = 2186 (C≡C), 1722 (C═O), 1649 (C═C), 1602, 1578 and 1558 (C═C, Ar). ^{1}H NMR (400 MHz, acetone-d_6) δ (ppm) 8.06–8.03 (m, 2H), 7.99–7.96 (m, 2H), 7.92–7.89 (m, 2H), 7.67–7.64 (m, 2H), 7.59–7.48 (m, 6H), 7.17 (td, J_1 = 1.4 Hz, J_2 = 0.7 Hz, 1H), 6.96 (d, J = 0.7 Hz, 1H), 6.77 (dd, J_1 = 2.0 Hz, J_2 = 1.0 Hz, 1H), 6.23 (d, J = 0.7 Hz, 1H), 3.91 (s, 3H), 1.76–1.68 (m, 2H), 1.41–1.31 (m, 6H), 0.88 (t, J = 7.0 Hz, 3H). ^{13}C NMR (100 MHz, $CDCl_3$) δ (ppm) 153.8, 151.4, 149.2, 143.3, 133.3, 133.1, 130.9, 129.8, 129.7, 129.4, 129.2, 129.0, 128.9, 128.8, 128.5, 127.0, 125.3, 124.7, 114.6, 108.6, 107.7, 102.9, 96.2, 87.0, 52.4, 31.8, 30.3, 29.7, 29.1, 22.8, 14.3. MS (MALDI) *m/z* 570.2 [$M^{+\cdot}$].

3.5.10. 4-((5-((2,6-diphenyl-4H-pyran-4-ylidene)methyl)-4-hexylthiophen-2-yl)ethynyl)benzoic acid (1b)

To a solution of ester **11b** (81 mg, 0.14 mmol) in anhydrous THF (3 mL), an aqueous solution of NaOH (16.8 mg, 3 equiv) was added dropwise and the reaction was stirred under argon at 40 °C for 31 h. The solvent was removed under reduced pressure. Then, the reaction was acidified to pH 2–3 with 15 mL of 1 M HCl and a red precipitate appears. The solid was filtered and washed first with EtOH/H_2O (9:1), then, cool hexane. (52 mg, 67%).

Mp (°C): 301–303. IR (KBr): ῡ (cm^{-1}) = 3442 (O–H), 2180 (C≡C), 1690 (C═O), 1653 (C═C), 1602, 1578 and 1555 (C═C, Ar). ^{1}H NMR (400 MHz, THF-d_8): δ (ppm) 8.02–8.00 (m, 2H), 7.91–7.89 (m, 2H), 7.84–7.82 (m, 2H), 7.56–7.38 (m, 8H), 7.15 (s, 1H), 6.83 (s, 1H), 6.63 (s, 1H), 6.13 (s, 1H), 2.77 (t, J = 7.6 Hz, 2H), 1.43–1.29 (m, 8H), 0.91–0.85 (m, 3H). ^{13}C NMR (100 MHz, THF-d_8) δ (ppm) 167.2, 154.9, 152.3, 149.9, 144.4, 134.3, 134.1, 131.6, 131.3, 130.8, 130.7, 130.1, 129.8, 129.6, 128.9, 127.9, 126.0, 125.5, 115.7, 109.5, 108.9, 103.5, 97.1, 87.1, 32.8, 31.3, 30.5, 30.1, 23.6, 14.6. HRMS (ESI^+) *m/z*: 579.1513 [M+Na]$^+$; calculated for $C_{37}H_{32}O_3SNa$: 579.1964.

3.5.11. Methyl 4-((5-((2,6-diphenyl-4H-pyran-4-ylidene)methyl)-4-hexylthiophen-2-yl)ethynyl)-2-(trifluoromethyl)benzoate (12b)

To a deoxygenated solution of **7b** (135.35 mg, 0.31 mmol), ester **10** (102 mg, 0.31 mmol), CuI (4 mg, 0.02 mmol) and $Pd(PPh_3)_2Cl_2$ (14.1 mg, 0.02 mmol) in anhydrous THF (10 mL), freshly distilled diisopropylamine (6 mL) was added dropwise under argon. After stirring 14 h at 60 °C, the reaction was cooled to room temperature and the solvent removed under vacuum. The crude product was filtered through a layer of silica gel with hexane/CH_2Cl_2 (1:1) as eluent and then, it was purified by centrifugal thin-layer chromatography on silica gel using hexane/CH_2Cl_2 (8:2) to afford **12b** as a red oil (99 mg, 50%).

IR (KBr): ῡ (cm^{-1}) = 2186 (C≡C), 1727 (C═O), 1654 (C═C), 1603, 1580 and 1558 (C═C, Ar). ^{1}H NMR (300 MHz, $CDCl_3$) δ (ppm) 7.89–7.74 (m, 6H), 7.71–7.66 (m, 1H), 7.54–7.37 (m, 6H), 7.13–7.11 (m, 1H), 6.74 (s, 1H), 6.43 (d, J = 2.2 Hz, 1H), 6.06 (s, 1H), 3.95 (s, 3H), 2.74 (t, J = 7.6 Hz, 2H), 1.76–1.62 (m, 2H), 1.43–1.26 (m, 6H), 0.93–0.84 (m, 3H). ^{19}F NMR (282 MHz, $CDCl_3$) δ (ppm) −59.92. ^{13}C NMR (100 MHz, $CDCl_3$) δ (ppm) 166.7, 153.9, 151.5, 149.8, 144.0, 133.5, 133.2, 133.1, 130.9, 129.8, 129.7, 129.6, 129.4, 129.2, 129.1 (q, J = 6.27 Hz), 128.9, 128.8, 127.6, 126.9, 125.2, 124.7, 123.2 (q, J = 273.6 Hz), 113.8, 108.6, 107.6, 102.8, 94.8, 88.1, 53.0, 31.8, 30.3, 29.7, 29.1, 22.8, 14.2. MS (MALDI) *m/z* 638.1 [$M^{+\cdot}$].

3.5.12. 4-((5-((2,6-diphenyl-4H-pyran-4-ylidene)methyl)-4-hexylthiophen-2-yl)ethynyl)-2 (trifluoromethyl)benzoic acid (2b)

To a solution of **12b** (38 mg, 0.059 mmol) in anhydrous THF (3 mL), an aqueous solution of NaOH (7.08 mg, 3 equiv) was added dropwise and the reaction was stirred under argon at 40 °C for 72 h. The solvent was removed under reduced pressure. Then, the reaction was acidified to pH 2–3 with 15 mL of 1 M HCl and a red precipitate appears. The solid was filtered and washed with a solution of hexane/CH_2Cl_2 (9:1) (17.1 mg, 46%).

Mp (°C): 174–179. IR (KBr): ῡ (cm^{-1}) = 3450 (O–H), 2175 (C≡C), 1709 (C═O), 1653 (C═C), 1602, 1579 and 1560 (C═C, Ar). ^{1}H NMR (300 MHz, CD_2Cl_2) δ (ppm) 7.98 (d, J = 8.1 Hz, 1H), 7.92–7.87 (m, 3H), 7.83–7.78 (m, 2H), 7.74 (dd, J_1 = 8.1 Hz, J_2 = 1.6 Hz, 1H), 7.53–7.43 (m, 6H), 7.15 (d, J = 2.0 Hz, 1H), 6.81 (s, 1H), 6.50 (d, J = 2.0 Hz, 1H), 6.10 (s, 1H), 2.77 (t, J = 7.6 Hz, 2H), 1.73–1.65 (m, 2H), 1.39–1.31 (m, 6H), 0.90 (t, J = 5.4 Hz, 3H). ^{13}C NMR (75 MHz, THF) δ (ppm) 167.2, 155.0, 152.4, 150.6, 145.0, 134.6, 134.2, 134.0, 133.2, 132.1, 131.8, 130.8, 130.4, 130.2, 129.8, 129.7, 129.6, 128.0, 127.8, 126.0, 125.5, 114.9, 109.4, 108.8, 103.4, 95.7, 88.1, 32.8, 31.3, 30.4, 30.1, 23.7, 14.6. ^{19}F NMR (376 MHz, CD_2Cl_2) δ −59.97. MS (MALDI) m/z 624.18 [$M^{+\cdot}$].

3.5.13. 4-(5-((2,6-diphenyl-4H-pyran-4-ylidene)methyl)-4-hexylthiophen-2-yl)-2 (trifluoromethyl)benzoic acid (3b)

This compound was synthesized in a three step synthetic route:

i) To a deoxygenated and argon purged solution of aldehyde **13b** (269 mg, 0.98 mmol) and (4-(methoxycarbonyl)-3-(trifluoromethyl) phenyl)boronic acid **14** (250 mg, 0.98 mmol) in ethanol (2 mL) and water (2 mL) was added $PdCl_2(PPh_3))_2$ (35 mg, 0.049 mmol) and Na_2CO_3 (262 mg, 2.47 mmol). The reaction mixture was deoxygenated again and heated at 110 °C for 16 h. Then, it was cooled to room temperature and solvents were removed under reduced pressure. The crude was quenched with water (10 mL), and extracted with ethyl acetate (3 × 30 mL). The organic layer was dried over $MgSO_4$. The obtained crude was purified by centrifugal thin-layer chromatography on silica gel with hexane to afford a red solid (70 mg). This solid was identified by ^{1}H NMR as a mixture of methyl 4-(5-formyl-4-hexylthiophen-2-yl)-2-(trifluoromethyl)benzoate (**15b**) and ethyl 4-(5-formyl-4-hexylthiophen-2-yl)-2-(trifluoromethyl)benzoate (**15'b**) (25/75), and it was used in the following step.

^{1}H NMR (300 MHz, CD_2Cl_2) δ (ppm) Hydrogens that appear in different signals for compounds **15b** and **15'b** are marked as bold; the rest of hydrogens appear in the same signal. 9.89 (s, 1.3H), 7.92–7.83 (m, 2.7H), 7.75–7.69 (m, 2.7H), **4.41 (q, J = 7.2 Hz, 2H)**, **3.95 (s, 1H)**, 2.70–2.61 (m, 2.7H), 1.66–1.59 (m, 2.8H), **1.39 (t, J = 7.1 Hz, 3H)**, 1.31–1.23 (m, 8.1H), 0.88–0.83 (m, 4.1H). ^{13}C NMR (75 MHz, CD_2Cl_2) δ 183.4, 169.4, 166.6, 145.2, 145.1, 143.2, 142.6, 139.0, 138.2, 137.5, 137.3, 132.9, 131.8, 131.5, 131.4, 129.8, 128.0, 125.6, 122.0, 62.8, 53.5, 32.0, 31.2, 31.0, 29.5, 29.4, 29.1, 23.1, 14.3. ^{19}F NMR (282 MHz, CD_2Cl_2) δ (ppm) −60.06, −59.73. MS (MALDI) m/z 398.1, 412.1.

ii) A solution of 2,6-diphenyl-(4*H*-pyran-4-ylidene)-diphenylphosphine oxide **4** (74 mg, 0.17 mmol) in 4 mL of anhydrous THF was prepared under argon and cooled to −78 °C. To this solution, *n*-BuLi 1.6 M in hexanes (125 μL, 0.2 mmol) was added dropwise and the mixture was stirred at −78 °C for 20 min. Then, a solution of the mixture **15b** + **15'b** (70 mg) in 4 mL of anhydrous THF was added dropwise, and the solution was warmed up to room temperature and stirred for 3 h. The reaction was quenched by the addition of aqueous saturated NH_4Cl solution, extracted with AcOEt (3 × 20 mL), and washed with water (3 × 20 mL). The organic phase was dried over $MgSO_4$ and the solvent was removed under reduced pressure. The crude was purified by centrifugal thin-layer chromatography on silica gel with hexane/ethyl acetate (9:1) to obtain a dark red solid. (74 mg). This solid was identified by ^{1}H NMR as a mixture of methyl 4-(5-((2,6-diphenyl-4*H*-pyran-4-ylidene)methyl)-4-hexylthiophen-2-yl)-2-(trifluoromethyl) benzoate (**16b**) and ethyl 4-(5-((2,6-diphenyl-4*H*-pyran-4-ylidene) methyl)-4-hexylthiophen-2-yl)-2-(trifluoromethyl)benzoate (**16'b**) (25/75), and it was used in the following step.

^{1}H NMR (300 MHz, CD_2Cl_2) δ (ppm) Hydrogens that appear in different signals for compounds **16b** and **16'b** are marked as bold; the rest of hydrogens appear in the same signal. 7.91–7.69 (m, 9.6H), 7.53–7.35 (m, 8H), 7.14 (dd, J = 2.0, 0.8 Hz, 1.3H), 6.91 (d, J = 0.8 Hz, 1.3H), 6.48 (dd, J = 2.0, 0.6 Hz, 1.3H), 6.10 (d, J = 0.8 Hz, 1.3H), **4.40 (q, J = 7.1 Hz, 2H), 3.94 (s, 1H)**, 2.71–2.64 (m, 2.7H), 1.72-1.61 (m, 2.8H), **1.40 (t, J = 7.1 Hz, 3H)**, 1.37–1.26 (m, 8.1H), 0.88–0.83 (m, 4.1H).

iii) To a solution of the mixture **16b** + **16'b** (74 mg) in anhydrous THF (3 mL), an aqueous solution of NaOH (18.9 mg) was added dropwise and the reaction was stirred under argon at 75 °C for 5 h. Then, the solution was cooled, and the solvent removed under reduced pressure. The crude was acidified with 10 mL of 1 M HCl, extracted with CH_2Cl_2 (2 × 30 ml), and finally washed with saturated NaCl solution. The organic layer was dried over anhydrous $MgSO_4$ and evaporated. The resulting solid was washed with H_2O/EtOH (9:1) to obtain **3b** as an orange solid. (46 mg, 8% overall the three steps).

Mp (°C): 177–179. IR (KBr): ῡ (cm^{-1}) = 3424 (O–H), 1711 (C═O), 1653 (C═C), 1602, 1579 and 1559 (C═C, Ar). ^{1}H NMR (400 MHz, CD_2Cl_2) δ (ppm) 7.97 (d, J = 8.1 Hz, 1H), 7.83 (d, J = 1.8 Hz, 1H), 7.80–7.73 (m, 2H), 7.73–7.64 (m, 3H), 7.44–7.29 (m, 6H), 7.05 (d, J = 2.0 Hz, 1H), 6.82 (s, 1H), 6.39 (d, J = 2.0 Hz, 1H), 6.00 (s, 1H), 2.63–2.56 (m, 2H), 1.59–1.57 (m, 2H), 1.35–1.14 (m, 6H), 0.82–0.76 (m, 3H). ^{13}C NMR (75 MHz, CD_2Cl_2) δ (ppm) 170.7, 154.0, 151.6, 142.7, 142.0, 140.1, 133.7, 133.5, 132.6, 132.2, 132.0, 130.2, 130.0, 129.8, 129.6, 129.3, 129.2, 127.6 (q, J = 5.0 Hz), 127.3, 125.6, 125.0, 108.9, 107.8, 103.1, 32.2, 31.3, 29.7, 29.5, 23.2, 14.4. ^{19}F NMR (282 MHz, CD_2Cl_2) δ −59.75. HRMS (ESI^-) m/z: 599.1862 [M − H]$^-$; calculated for $C_{36}H_{30}F_3O_3S$: 599.1873.

4. Conclusions

In summary, five novel dyes based on 4*H*-pyranylidene as donor moiety, including an ethynyl group and a benzoic acid with or without a trifluoromethyl group to modulate the acceptor properties of the sensitizers have been synthesized and studied.

In this series, a great tendency to form aggregates is observed, probably due to high degree of planarity of the dyes, enhanced by the presence of the triple bond. Therefore, the use of an antiaggregant is necessary to obtain moderate efficiencies.

The results obtained allow to conclude that, in general, the inclusion of the CF_3 group and the hexyl chain in the thiophene core lead to an increase in the efficiency value.

Moreover, the presence of a trifluoromethyl group tends to reduce both the recombination processes and the dye load on the electrode, improving the V_{oc} values. On the other hand, the CF_3 group enhances the molar extinction coefficients (slightly if a hexyl chain decorates the thiophene spacer), without altering the oxidation potential values.

The studied dyes have a better response under indoor conditions, leading to an increase of the efficiency: 36% for compound **2b**, having in its structure a hexyl chain in the thiophene ring and the CF_3 group.

All these observations indicate that, with a careful design of the molecular structure, the incorporation of a trifluoromethyl group can be promising for future more efficient sensitizers.

CRediT authorship contribution statement

Raquel Royo: Investigation, Methodology, Writing – original draft,

Writing – review & editing. **Amelia Domínguez-Celorrio:** Investigation, Methodology. **Santiago Franco:** Investigation, Conceptualization, Validation, Writing – original draft, Writing – review & editing, Supervision. **Raquel Andreu:** Conceptualization, Validation, Writing – original draft, Writing – review & editing, Supervision, Funding acquisition. **Jesús Orduna:** Methodology, Formal analysis.

Declaration of competing interest

The authors declare that they have no known competing financial interests or personal relationships that could have appeared to influence the work reported in this paper.

Acknowledgments

Financial support from Ministerio de Ciencia e Innovación (PID2019-104307 GB-I00/AEI/10.13039/501100011033) and Gobierno de Aragón-FEDER-Fondo Social Europeo (E47_20R) is gratefully acknowledged. R. Royo acknowledges for the financial support of Gobierno de Aragón: Fellowship program 2018–2022 period co-financed with the Operational Program FSE Aragón 2014-202. We thank Dr. B. Villacampa (University of Zaragoza, Spain) for helpful discussions. Authors would like to acknowledge the use of Servicio General de Apoyo a la Investigación-SAI, Universidad de Zaragoza.

Appendix A. Supplementary data

Supplementary data to this article can be found online at https://doi.org/10.1016/j.dyepig.2022.110566.

References

[1] Hagfeldt A, Boschloo G, Sun L, Kloo L, Pettersson H. Dye-sensitized solar cells. Chem Rev 2010;110(11):6595–663.
[2] Kokkonen M, Talebi P, Zhou J, Asgari S, Soomro SA, Elsehrawy F, et al. Advanced research trends in dye-sensitized solar cells. J Mater Chem A 2021;9(17):10527–45.
[3] Gong J, Sumathy K, Qiao Q, Zhou Z. Review on dye-sensitized solar cells (DSSCs): advanced techniques and research trends. Renew Sustain Energy Rev 2017;68(Part_1):234–46.
[4] Kakiage K, Aoyama Y, Yano T, Oya K, Fujisawa J-i, Hanaya M. Highly-efficient dye-sensitized solar cells with collaborative sensitization by silyl-anchor and carboxy-anchor dyes. Chem Commun 2015;51(88):15894–7.
[5] Yella A, Lee H-W, Tsao HN, Yi C, Chandiran AK, Nazeeruddin MK, et al. Porphyrin-sensitized solar cells with cobalt (II/III)–Based redox electrolyte exceed 12 percent efficiency. Science 2011;334:629–34.
[6] Zhang D, Stojanovic M, Ren Y, Cao Y, Eickemeyer FT, Socie E, et al. A molecular photosensitizer achieves a Voc of 1.24 V enabling highly efficient and stable dye-sensitized solar cells with copper(II/I)-based electrolyte. Nat Commun 2021;12(1):1777.
[7] Ji J-M, Zhou H, Eom YK, Kim CH, Kim HK. 14.2% efficiency dye-sensitized solar cells by Co-sensitizing novel thieno[3,2-b]indole-based organic dyes with a promising porphyrin sensitizer. Adv Energy Mater 2020;10(15):2000124.
[8] Selvaraj P, Ghosh A, Mallick TK, Sundaram S. Investigation of semi-transparent dye-sensitized solar cells for fenestration integration. Renew Energy 2019;141:516–25.
[9] Godfroy M, Liotier J, Mwalukuku VM, Joly D, Huaulmé Q, Cabau L, et al. Benzothiadiazole-based photosensitizers for efficient and stable dye-sensitized solar cells and 8.7% efficiency semi-transparent mini-modules. Sustain Energy Fuels 2021;5(1):144–53.
[10] Barichello J, Vesce L, Mariani P, Leonardi E, Braglia R, Di Carlo A, et al. Stable semi-transparent dye-sensitized solar modules and panels for greenhouse application. Energies 2021;14(19).
[11] Freitag M, Teuscher J, Saygili Y, Zhang X, Giordano F, Liska P, et al. Dye-sensitized solar cells for efficient power generation under ambient lighting. Nat Photonics 2017;11(6):372–8.
[12] Devadiga D, Selvakumar M, Shetty P, Santosh MS. Dye-sensitized solar cell for indoor applications: a mini-review. J Electron Mater 2021;50:3187–206.
[13] Jiang ML, Wen J-J, Chen Z-M, Tsai W-H, Lin T-C, Chow TJ, et al. High-performance organic dyes with electron-deficient quinoxalinoid heterocycles for dye-sensitized solar cells under one sun and indoor light. ChemSusChem 2019;12(15):3654–65.
[14] Mishra A, Fischer MKR, Bäuerle P. Metal-free organic dyes for dye-sensitized solar cells: from structure: property relationships to design rules. Angew Chem-Int Ed. 2009;48(14):2474–99.
[15] Yahya M, Bouziani A, Ocak C, Seferoğlu Z, Sillanpää M. Organic/metal-organic photosensitizers for dye-sensitized solar cells (DSSC): recent developments, new trends, and future perceptions. Dyes Pigments 2021;192:109227.
[16] Zhang L, Cole JM. Anchoring groups for dye-sensitized solar cells. ACS Appl Mater Interfaces 2015;7(6):3427–55.
[17] Andreu R, Carrasquer L, Franco S, Garín J, Orduna J, Martínez de Baroja N, et al. 4H-Pyran-4-ylidenes: strong proaromatic donors for organic nonlinear optical chromophores. J Org Chem 2009;74(17):6647–57.
[18] Achelle S, Malval J-P, Aloïse S, Barsella A, Spangenberg A, Mager L, et al. Synthesis, photophysics and nonlinear optical properties of stilbenoid pyrimidine-based dyes bearing methylenepyran donor groups. ChemPhysChem 2013;14(12):2725–36.
[19] Marco AB, Martínez de Baroja N, Franco S, Garín J, Orduna J, Villacampa B, et al. Dithienopyrrole as a rigid alternative to the bithiophene π relay in chromophores with second-order nonlinear optical properties. Chem Asian J 2015;10(1):188–97.
[20] Solanke P, Achelle S, Cabon N, Pytela O, Barsella A, Caro B, et al. Proaromatic pyranylidene chalcogen analogues and cyclopenta[c]thiophen-4,6-dione as electron donors and acceptor in efficient charge-transfer chromophores. Dyes Pigments 2016;134:129–38.
[21] Tejeda-Orusco V, Andreu R, Orduna J, Villacampa B, Franco S, Civera A. Twisted one-dimensional charge transfer and related Y-shaped chromophores with a 4H-pyranylidene donor: synthesis and optical properties. J Org Chem 2021;86(4):3152–63.
[22] Tejeda-Orusco V, Blais M, Cabanetos C, Blanchard P, Andreu R, Franco S, et al. 4H-pyranylidene-based small push-pull chromophores: synthesis, structure, electronic properties and photovoltaic evaluation. Dyes Pigments 2020;178:108357.
[23] Poronik YM, Hugues V, Blanchard-Desce M, Gryko DT. Octupolar merocyanine dyes: a new class of nonlinear optical chromophores. Chem Eur J 2012;18(30):9258–66.
[24] Shen C, Courté M, Krishna A, Tang S, Fichou D. Quinoidal 2,2′,6,6′-tetraphenyl-dipyranylidene as a dopant-free hole-transport material for stable and cost-effective perovskite solar cells. Energy Technol 2017;5(10):1852–8.
[25] Wang X, Guo Z, Zhu S, Liu Y, Shi P, Tian H, et al. Rational design of novel near-infrared fluorescent DCM derivatives and their application in bioimaging. J Mater Chem B 2016;4(27):4683–9.
[26] Bolag A, Nishida J-i, Hara K, Yamashita Y. Dye-sensitized solar cells based on novel diphenylpyran derivatives. Chem Lett 2011;40(5):510–1.
[27] Franco S, Garin J, Martinez De Baroja N, Perez-Tejada R, Orduna J, Yu Y, et al. New D-pi-A-conjugated organic sensitizers based on 4H-Pyran-4-ylidene donors for highly efficient dye-sensitized solar cells. Org Lett 2012;14(3):752–5.
[28] Gauthier S, Robin-Le Guen F, Wojcik L, Le Poul N, Planchat A, Pellegrin Y, et al. Synthesis and properties of novel pyranylidene-based organic sensitizers for dye-sensitized solar cells. Dyes Pigments 2019;171:107747.
[29] Gauthier S, Robin-le Guen F, Wojcik L, Le Poul N, Planchat A, Pellegrin Y, et al. Comparative studies of new pyranylidene-based sensitizers bearing single or double anchoring groups for dye-sensitized solar cells. Sol Energy 2020;205:310–9.
[30] Bolag A, Nishida J-i, Hara K, Yamashita Y. Enhanced performance of dye-sensitized solar cells with novel 2,6-diphenyl-4H-pyranylidene dyes. Org Electron 2012;13(3):425–31.
[31] Pérez Tejada R, Pellejà L, Palomares E, Franco S, Orduna J, Garín J, et al. Novel 4H-pyranylidene organic dyes for dye-sensitized solar cells: effect of different heteroaromatic rings on the photovoltaic properties. Org Electron 2014;15(11):3237–50.
[32] Pérez-Tejada R, Martínez de Baroja N, Franco S, Pellejà L, Orduna J, Andreu R, et al. Organic sensitizers bearing a trialkylsilyl ether group for liquid dye sensitized solar cells. Dyes Pigments 2015;123:293–303.
[33] Marco AB, Martínez de Baroja N, Andrés-Castán JM, Franco S, Andreu R, Villacampa B, et al. Pyranylidene/thienothiophene-based organic sensitizers for dye-sensitized solar cells. Dyes Pigments 2019;161:205–13.
[34] Andrés-Castán JM, Andreu R, Villacampa B, Orduna J, Franco S. 4H-pyranylidene organic dyes for dye-sensitized solar cells: twisted structures towards enhanced power conversion efficiencies. Sol Energy 2019;193:74–84.
[35] Koumura N, Wang Z-S, Mori S, Miyashita M, Suzuki E, Hara K. Alkyl-functionalized organic dyes for efficient molecular photovoltaics. J Am Chem Soc 2006;128(44):14256–7.
[36] Teng C, Yang X, Yang C, Tian H, Li S, Wang X, et al. Influence of triple bonds as π-spacer units in metal-free organic dyes for dye-sensitized solar cells. J Phys Chem C 2010;114(25):11305–13.
[37] An J, Yang X, Cai B, Zhang L, Yang K, Yu Z, et al. Fine-tuning by triple bond of carbazole derivative dyes to obtain high efficiency for dye-sensitized solar cells with copper electrolyte. ACS Appl Mater Interfaces 2020;12(41):46397–405.
[38] Gao Y, Li X, Hu Y, Fan Y, Yuan J, Robertson N, et al. Effect of an auxiliary acceptor on D–A–π–A sensitizers for highly efficient and stable dye-sensitized solar cells. J Mater Chem A 2016;4(33):12865–77.
[39] Wu Y, Zhu W-H, Zakeeruddin SM, Grätzel M. Insight into D–a–π–A structured sensitizers: a promising route to highly efficient and stable dye-sensitized solar cells. ACS Appl Mater Interfaces 2015;7(18):9307–18.
[40] Shen L, Yang X, An J, Zhang L, Yang K, Deng Z. Effect of different site trifluoromethylbenzoic acid organic photosensitizer for dye-sensitized solar cells. ChemistrySelect 2021;6(19):4645–50.
[41] Reddy KSK, Chen Y-C, Wu C-C, Hsu C-W, Chang Y-C, Chen C-M, et al. Cosensitization of structurally simple porphyrin and anthracene-based dye for dye-sensitized solar cells. ACS Appl Mater Interfaces 2018;10(3):2391–9.
[42] Tsai M-C, Wang C-L, Chang C-W, Hsu C-W, Hsiao Y-H, Liu C-L, et al. A large, ultra-black, efficient and cost-effective dye-sensitized solar module approaching 12%

overall efficiency under 1000 lux indoor light. J Mater Chem A 2018;6(5):1995–2003.
[43] Biswas S, Kim H. Solar cells for indoor applications: progress and development. Polymers 2020;12(6):1338.
[44] Michaels H, Rinderle M, Freitag R, Benesperi I, Edvinsson T, Socher R, et al. Dye-sensitized solar cells under ambient light powering machine learning: towards autonomous smart sensors for the internet of things. Chem Sci 2020;11(11):2895–906.
[45] Liu IP, Lin W-H, Tseng-Shan C-M, Lee Y-L. Importance of compact blocking layers to the performance of dye-sensitized solar cells under ambient light conditions. ACS Appl Mater Interfaces 2018;10(45):38900–5.
[46] Venkatesan S, Liu IP, Tseng Shan C-M, Teng H, Lee Y-L. Highly efficient indoor light quasi-solid-state dye sensitized solar cells using cobalt polyethylene oxide-based printable electrolytes. Chem Eng J 2020;394:124954.
[47] Abaev V, Karsanov I, Urtaeva Z, Blinokhvatov A, Bumber A, Okhlobystin O. Production and properties of (4*H*-pyran-4-yl)diphenylphosphine oxides. Zh Obshch Khim 1990;60:1012–9.
[48] Zhan H, Lamare S, Ng A, Kenny T, Guernon H, Chan W-K, et al. Synthesis and photovoltaic properties of new metalloporphyrin-containing polyplatinyne polymers. Macromolecules 2011;44(13):5155–67.
[49] Wang Y, Xu L, Wei X, Li X, Ågren H, Wu W, et al. 2-Diphenylaminothiophene as the donor of porphyrin sensitizers for dye-sensitized solar cells. New J Chem 2014;38(7):3227–35.
[50] Bylund J, Ek M, Holenz J, Johansson MH, Kers A, Närhi K, et al. WO 2009/064250 A1, 2009.
[51] Suzuki T, Ota Y, Ri M, Bando M, Gotoh A, Itoh Y, et al. Rapid discovery of highly potent and selective inhibitors of histone deacetylase 8 using click chemistry to generate candidate libraries. J Med Chem 2012;55(22):9562–75.
[52] Although compound 10 has been previously reported by other synthetic methods: See [a)] Shi G, Shao C, Pan S, Yu J, Zhang Y. Org Lett 2015;17:38–41.[b)] Yang B, Yu D, Xu X-H, Qing F-L. ACS Catal 2018;4. 2839–43, for this work, it has been synthesized as ester from the corresponding benzoic acid derivative 8 and methanol in acid medium. See Experimental section.
[53] Conditions for the Suzuki coupling:, Barbosa AJ. Preparation of heterocyclic integrin agonists for treatment of cancer. 2018. WO2018126072A1.
[54] Wang Z-S, Cui Y, Dan-oh Y, Kasada C, Shinpo A, Hara K. Thiophene-functionalized coumarin dye for efficient dye-sensitized solar cells: electron lifetime improved by coadsorption of deoxycholic acid. J Phys Chem C 2007;111(19):7224–30.
[55] Zhou G, Pschirer N, Schöneboom JC, Eickemeyer F, Baumgarten M, Müllen K. Ladder-type pentaphenylene dyes for dye-sensitized solar cells. Chem Mater 2008;20(5):1808–15.
[56] Lin L-Y, Tsai C-H, Wong K-T, Huang T-W, Hsieh L, Liu S-H, et al. Organic dyes containing coplanar diphenyl-substituted dithienosilole core for efficient dye-sensitized solar cells. J Org Chem 2010;75(14):4778–85.
[57] Tian H, Sun L. Iodine-free redox couples for dye-sensitized solar cells. J Mater Chem 2011;21(29):10592–601.
[58] Grätzel M. Photoelectrochemical cells. Nature 2001;414(6861):338–44.
[59] Wang Q, Moser J-E, Grätzel M. Electrochemical impedance spectroscopic analysis of dye-sensitized solar cells. J Phys Chem B 2005;109(31):14945–53.
[60] Kern R, Sastrawan R, Ferber J, Stangl R, Luther J. Modeling and interpretation of electrical impedance spectra of dye solar cells operated under open-circuit conditions. Electrochim Acta 2002;47(26):4213–25.
[61] Bertoluzzi L, Ma S. On the methods of calculation of the charge collection efficiency of dye sensitized solar cells. PhysChemChemPhys 2013;15(12):4283–5.